

## Size-of-Source Effect Sensitivities in Radiometers

M. R. Dury · T. C. Arneil · G. Machin ·  
T. M. Goodman

Received: 29 July 2013 / Accepted: 23 June 2014 / Published online: 18 July 2014  
© Crown Copyright 2014

**Abstract** When performing high accuracy radiation thermometry, the size-of-source effect (SSE) of a radiometer can provide a significant contribution to the uncertainties associated with the measurements. During the development of a new radiometer designed specifically to measure the melting points of high-temperature fixed-point cells, indirect SSE measurements were performed on a prototype instrument to aid selection of optical components and their optimum positions with the aim of minimizing its SSE. As the radiometer's objective lens can produce much of the scattered light that contributes to the SSE, a set of objective lenses was compared and found to have SSEs between  $7 \times 10^{-4}$  and  $<6 \times 10^{-5}$ . Further improvements were found by controlling the positioning and size of the stray light reducing Lyot stop. The diameter of the Lyot stop had to be set carefully: too small a diameter and it provides a low SSE but reduces the instrument's signal from the source; too large a diameter and it provides little or no reduction in the SSE. The sensitivities in the Lyot stop and collimating lens positions were tested, and the instrument's SSE was found to be tolerant of small displacements of either the lens or Lyot stop, however, larger movements yielded an increase in the SSE. The extremes in position increased the SSE to  $3 \times 10^{-4}$  for the collimating lens and  $4 \times 10^{-4}$  for the Lyot stop.

**Keywords** High-temperature fixed-points · Lyot stop · Radiation thermometer · Radiometer · Size-of-source effect

---

M. R. Dury (✉) · G. Machin · T. M. Goodman  
National Physical Laboratory, Teddington, United Kingdom  
e-mail: martin.dury@npl.co.uk

T. C. Arneil  
University of Cambridge, Cambridge, UK

## 1 Introduction

The National Physical Laboratory (NPL) is currently developing a new radiometer [1] specifically to measure the melting temperatures of high-temperature fixed-point (HTFP) cells [2]. This work stems from the HTFP measurements that NPL undertook in 2009 for Workpackage 4 (WP4) of the Comité Consultatif de Thermométrie Working Group 5 (CCT WG 5) HTFP Research Plan. WP4 has the aim of assessing and improving the absolute thermometry capability of participating laboratories [3]. Upon its completion, participating laboratories reported values and associated uncertainties for the melting temperatures that they had measured to the coordinating institute. Participants also reported observations and improvements that could be applied to the next stage of measurements, Workpackage 5, which has the aim of assigning definitive values for the melting temperatures of these HTFPs, with the lowest possible uncertainties [4]. NPL's WP4 report suggested developing a new radiometer to achieve this aim.

During WP4, NPL used the absolute radiation thermometer (ART) to measure the HTFP cells [5]. This radiometer was designed approximately 10 years ago as a simple radiometer system and comprises two calibrated apertures at a known distance, a singlet lens and a filter radiometer. However, the ART had a large size-of-source effect (SSE) due to its simple design [1]. Furthermore, because the ART was calibrated using the hybrid method [6], the correction of the SSE required an estimate of the response to an infinite source which is difficult to determine experimentally.

A radiance mode instrument has two advantages. First, the SSE correction is calculated from a combination of the instrument SSE and the radial radiance distribution of the calibration source and HTFP furnaces, rather than needing an estimate to an infinite source, and second, an instrument can be developed with additional optical elements that reduce the SSE so it is negligible [7,8].

On this understanding, NPL is building a new radiometer, the “Thermodynamic Optical Radiometer” (THOR), which is based on the optical design described by Yoon et al. [9], specifically to measure the melting points of HTFP cells. This paper describes initial investigations in THOR's development, using “indirect method” [10] SSE measurements to identify an objective lens with a low SSE. Further measurements to understand how the radiometer's additional optical components can affect its SSE are also described.

## 2 Experimental Setup

### 2.1 The Thermodynamic Optical Radiometer Prototype

THOR [1] comprises a 50.8 mm diameter objective achromatic doublet lens, which is stopped to 40 mm by a silicon nitride objective aperture; it has a focal length of 200 mm, such that when the HTFP aperture is positioned 500 mm from the objective lens, an image is focussed on the field stop which is located 333 mm from the objective lens, inside the radiometer. The image magnification is 2:3, so that the 1 mm diameter field stop defines an imaged area of 1.5 mm onto the HTFP aperture, which has a 3 mm

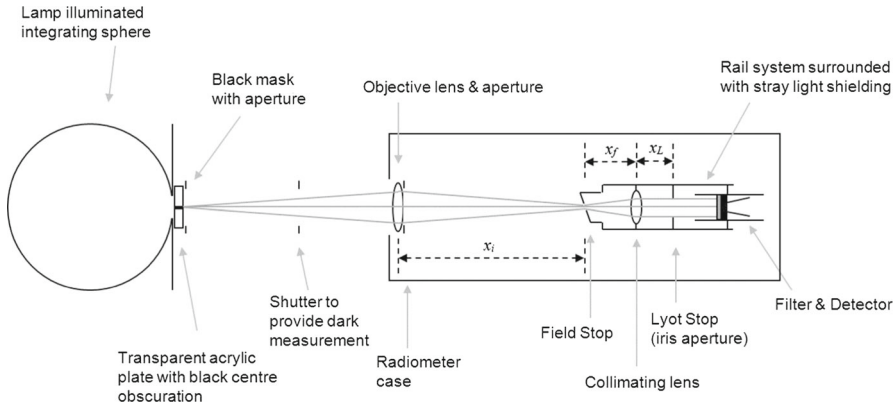


**Fig. 1** General measurement setup for all of the experiments described in this paper. The radiometer prototype is aligned with the sphere, such that a focussed image of the blackened cavity is formed at the field stop

diameter. The field stop is aligned at a 10° angle and highly polished to reflect incident light that does not pass through its aperture onto a mirror that is directed towards an internal telescope, enabling THOR to be aligned by eye. To reduce THOR’s SSE, a collimating lens is positioned 50 mm behind the field stop aperture and a 6 mm Lyot stop is placed 57.5 mm behind the collimating lens. A prototype radiometer based on these specifications was built in order to conduct experiments to identify the optimum optical components for THOR and to investigate their SSE sensitivities.

### 2.2 SSE Measurement Setup

The radiance source used for the SSE measurements comprised a 250 mm diameter integrating sphere, illuminated by a tungsten filament lamp, with a 60 mm diameter output port. A transparent acrylic plate that incorporated a 3 mm diameter blackened cavity provided an approximation to the aperture of a HTFP cavity. The prototype radiometer did not have an internal telescope and was aligned centrally with the plate’s blackened cavity, such that a focussed image of the cavity was formed at an unpolished field stop, as depicted in Fig. 1. SSE measurements were performed using the “indirect method” described in [10].

$$SSE \sigma (d) = \frac{(L_m - d_k)}{(L_0 - d_k)}. \tag{1}$$

Measurements of the SSE were carried out using the same type of 800 nm interference filter and 10 mm by 10 mm silicon detector that were later installed in THOR, and using 14 source apertures (with diameters,  $d$ , ranging from 2 mm to 50 mm), with and without the blackened cavity in place. From these measurements, the SSE was calculated using Eq. 1 [9], where the SSE  $\sigma(d)$  is the SSE for a particular sphere aperture diameter;  $L_m$  is the measurement of the sphere with the obscuring cavity and

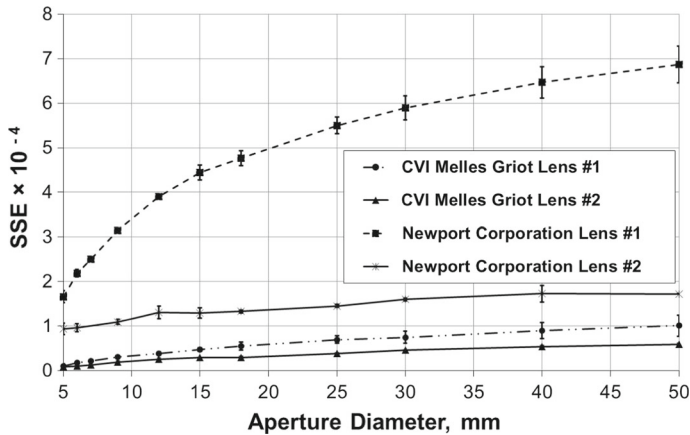


**Fig. 2** SSE produced from two batches of two objective lenses from different manufacturers and in different orientations. *Abscissa* shows the diameter of the sphere aperture. *Error bars* show measurement repeatability

with sphere aperture in place; and  $d_k$  is the dark measurement (measured with the radiometer's view of the sphere port blocked using the shutter);  $L_0$  is a measurement of the sphere without the obscuring cavity, but with the sphere aperture in place.

### 3 Results

#### 3.1 Objective Lens Comparison

The SSE of the radiometer was determined for different objective lenses, using a Lyot stop diameter of 6 mm. Only achromatic doublet lenses have been considered for use in THOR, due to their superior image quality when compared with singlet lenses. The lenses were chosen to match the requirements of the radiometer's objective lens, with focal lengths of 200 mm to produce the intended 2:3 magnification, and anti-reflective coatings aligning with the peak transmittance of the radiometer's 800 nm interference filter. The SSE of the instrument was compared using Newport Corporation (part number: PAC32AR.16) and CVI Melles Griot (part number: LAO-200.0-50.0-780-850) lenses as the instrument's objective lens, with two of each lens type measured. A Newport Corporation plano-convex singlet lens (part number: SPX016AR.16) was installed as the radiometer's collimating lens for all of the experiments described in this paper.

The SSE results from both pairs of lenses are presented in Fig. 2. The CVI Melles Griot lenses are shown to have superior SSE performance to the Newport Corporation lenses for this application. A maximum SSE of  $7 \times 10^{-4}$  was recorded for Newport Corporation lens #1, while CVI Melles Griot lens #2 yielded the lowest overall maximum SSE of  $<6 \times 10^{-5}$  and was therefore chosen as THOR's objective lens and used as the prototype's objective lens for the other experiments described in this paper. The discrepancy between the lenses is difficult to explain without a much closer examination of their structure. However, as the manufacturer's specifications state identical

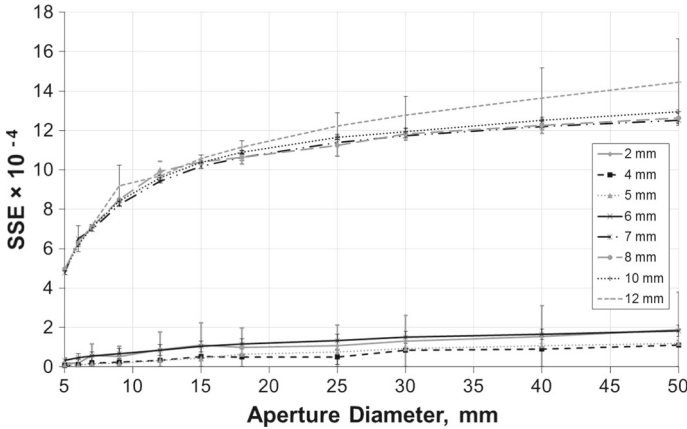


**Fig. 3** Effect of different Lyot stop diameters (2 mm, 4 mm, 5 mm, 6 mm, 7 mm, 8 mm, 10 mm, and 12 mm) on the SSE of the instrument when viewing the 3 mm diameter blackened cavity on the integrating sphere. *Abscissa* shows the sphere aperture diameter. *Error bars* show measurement repeatability. Lyot stop diameters of 6 mm or less are grouped within the lower portion of the graph; Lyot stop diameters greater than 6 mm are grouped within the upper portion of the graph

scratch-dig values (60-40) for both lens types, the difference in measured SSE values may have been caused by scatter from anomalies within the lenses or from the different cements (or bubbles in the cement) that adhere the component lenses together.

### 3.2 Lyot Stop Diameter Sensitivity

The optimum Lyot stop diameter for such a radiometer is determined from Eq. 2, which gives the demagnification factor,  $M$ , of the optical system. The parameters:  $x_i$ , the image distance of the objective lens or the distance from the objective lens to the field stop;  $x_f$ , the focal length of the collimating lens; and  $x_L$ , the image distance or the Lyot stop distance from the collimating lens [9], are depicted in Fig. 1.

$$M = \frac{x_i + x_f}{x_L} \tag{2}$$

Applying the parameters described in Sect. 2.1 to this equation, the optimum Lyot stop diameter for THOR is 6.66 mm. To measure the sensitivity of THOR’s SSE to the diameter of the Lyot stop, SSE measurements were performed on the prototype instrument with Lyot stop diameters of approximately 2 mm, 4 mm, 5 mm, 6 mm, 7 mm, 8 mm, 10 mm, and 12 mm.

Figure 3 shows the results of these measurements, presenting a stark difference in the SSE between Lyot stop diameters of 6 mm and 7 mm and those of larger diameter. For diameters of 7 mm or more, the Lyot stop diameter is too large to be effective, so the measured SSE is approximately five times greater than that for diameters of 6 mm or less.

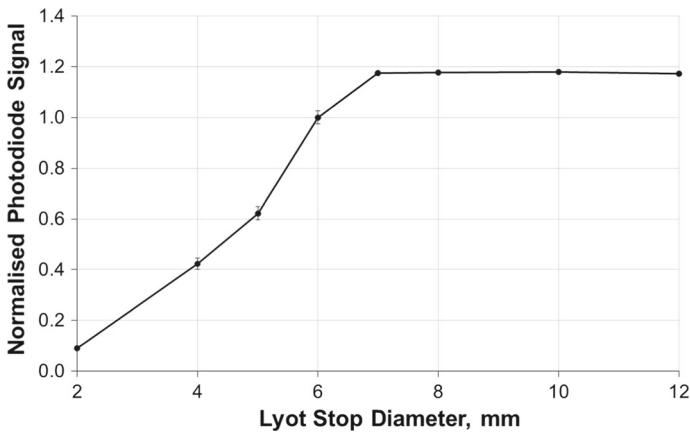


**Fig. 4** Measured radiometer signal against the Lyot stop diameter. Measured signals have been normalized against values measured for a Lyot stop diameter of 6 mm. Error bars depict measurement repeatability

By reducing the Lyot stop diameter, the light signal received by the instrument's detector was also reduced. This is confirmed in Fig. 4, which shows the signal for each Lyot stop diameter when the radiometer measured the sphere directly (without the cavity or source apertures in place); each signal value has been normalized against the 6 mm Lyot stop signal. The graph suggests that the 6 mm diameter Lyot stop is a reasonable compromise between reducing the radiometer's SSE and maximizing the measured signal. A Lyot stop diameter of 7 mm or greater does little to reduce the SSE, shown by the consistency of the SSE values for diameters of 7 mm, 8 mm, 10 mm, and 12 mm. A Lyot stop diameter smaller than 6 mm will reduce the SSE, but also the measured signal. This means that for Lyot stop diameters of around 6 mm and smaller, the Lyot stop becomes one of the defining apertures of the instrument. Therefore, as the Lyot stop diameter decreases, the instrument will become sensitive to the stability of the Lyot stop diameter.

### 3.3 Lyot Stop Position Sensitivity

An aperture forms a Lyot stop within a radiometer when it is positioned at the image of the objective aperture that is formed by the collimating lens. Stray light from the objective lens that passes through the field stop, will do so at a sharper angle than the rays forming the image of the target (the HTFP aperture), and will be spread to the outer edge of the image formed by the collimating lens. The ideal Lyot stop is slightly smaller than the image of the objective lens, and will therefore block this stray light, while allowing the parallel beam that forms the image of the target to pass into the detector; this idealized situation is depicted in Fig. 5a.

Equation 3 gives the optimum distance of the Lyot stop from the collimating lens [9], such that the objective lens is imaged onto the Lyot stop:

$$\frac{1}{x_i + x_f} + \frac{1}{x_L} = \frac{1}{x_f}. \quad (3)$$

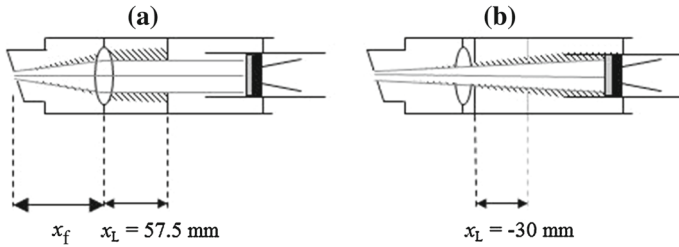


**Fig. 5** Diagram to show how the Lyot stop position can affect the SSE of the radiometer when viewing the 3 mm diameter blackened cavity on the integrating sphere. Stray light from the objective lenses is represented by the shaded region

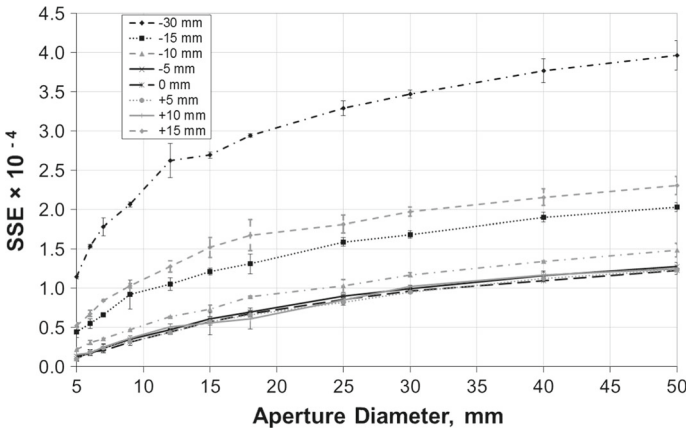


**Fig. 6** SSE of the radiometer viewing the 3 mm diameter blackened cavity on the integrating sphere with different Lyot stop positions. Abscissa shows the diameter of the sphere aperture. Error bars show measurement repeatability. Lyot stop displacements of 0 mm,  $\pm 5$  mm, and  $+10$  mm are grouped within the lower portion of the graph

For a radiometer with THOR’s geometry, the image of the objective lens is formed at 57.5 mm; this is the optimum position for the Lyot stop. When moved away from this optimum position, the aperture no longer behaves as a Lyot stop. To understand the instrument’s sensitivities to this misalignment, SSE measurements were performed using the radiometer with the Lyot stop moved by  $\pm 5$  mm,  $\pm 10$  mm,  $\pm 15$  mm, and  $-30$  mm from the default position of 57.5 mm.

The results of this experiment are shown in Fig. 6. For small Lyot stop displacements of  $\pm 5$  mm, and  $+10$  mm from the default position, there is no measurable change in the instrument’s SSE. Despite the slight beam divergence produced in the non-idealized situation, due to the fact that the field stop is not a point source, when the Lyot stop is in its optimum position (or only a small distance away from it) it will still prevent stray light from reaching the detector. As the results for  $-10$  mm,  $-15$  mm, and  $-30$  mm displacements show, if the Lyot stop is moved too close to the collimating lens then the radiometer’s SSE will increase; for the  $-30$  mm displacement, a maximum SSE of  $4 \times 10^{-4}$  was recorded. In this situation the Lyot stop ceases to be effective and

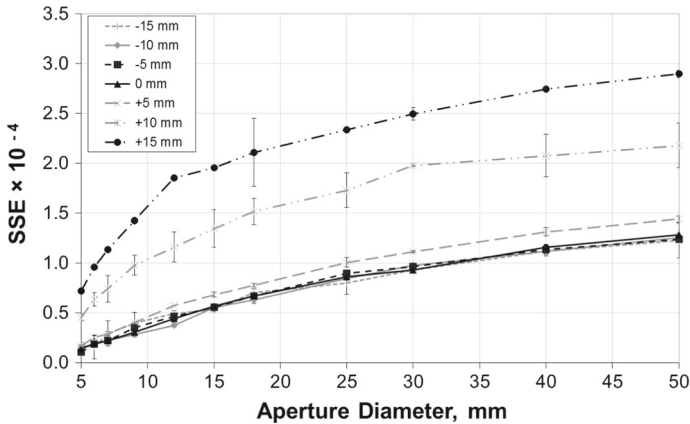


**Fig. 7** SSE of the radiometer viewing the 3 mm diameter blackened cavity on the integrating sphere with different collimating lens positions. *Abscissa* shows the diameter of the sphere aperture. *Error bars* show measurement repeatability. Collimating lens positions of 0 mm,  $\pm 5$  mm, and  $\pm 10$  mm are grouped within the lower portion of the graph

allows stray light from the slightly divergent beam to reach the detector as depicted in Fig. 5b.

Figure 6 also shows an increase in the SSE for a Lyot stop position of  $+15$  mm, where the Lyot stop has been moved as close as possible to the detector (there was not sufficient room for a  $+30$  mm measurement). This could be due to inter-reflections, possibly from the surface of the interference filter.

### 3.4 Collimating Lens Position Sensitivity

To produce a parallel beam of light from the field stop, the collimating lens should be placed behind the field stop at a distance equal to its focal length. As the collimating lens will be aligned by eye, it may be difficult to judge when the beam is exactly collimated. Therefore, to determine the instrument's SSE sensitivities to the lens position, measurements were performed using the radiometer with the collimating lens moved by  $\pm 5$  mm,  $\pm 10$  mm, and  $\pm 15$  mm from its optimum position, 50 mm from the field stop.

As Fig. 7 shows, there is no measurable change in the radiometer's SSE as the collimating lens is moved closer to the field stop ( $-5$  mm,  $-10$  mm, and  $-15$  mm). Figure 8a suggests an explanation, showing the situation where the collimating lens is moved closer to the field stop and produces an increasingly divergent beam of light. In this case the Lyot stop, in its optimum position, not only blocks the stray light but also blocks some of the 'wanted' light. The overall signal of the radiometer decreased as the distance of the lens from the field stop was decreased, consistent with this explanation. Figure 8b depicts the collimating lens in its ideal position; where its distance from the field stop is equal to its focal length, such that it produces a parallel beam of light and only the stray light is blocked.



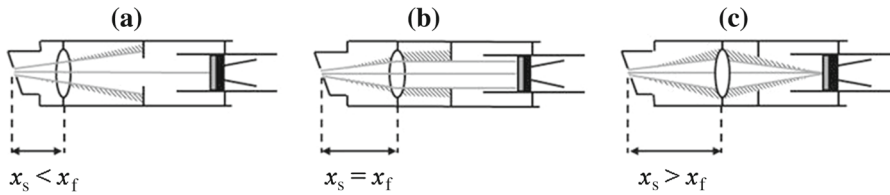


**Fig. 8** Schematic diagram showing how the collimating lens position can affect the radiometer's SSE, where  $x_s$  is the distance between the field stop and the collimating lens and  $x_f$  is the collimating lens' focal length. Stray light caused by the instrument's SSE from the objective lenses is represented by the *shaded region*

The graph in Fig. 7 also shows the measured SSE increasing with the distance of the collimating lens from the field stop (+5 mm, +10 mm, and +15 mm); for the +15 mm displacement a SSE of  $3 \times 10^{-4}$  was recorded. Figure 8c suggests an explanation, showing the lens focusing the light collected from the field stop as the distance of the lens from the field stop is increased. This forms a divergent beam that allows stray light to pass through the Lyot stop and reach the detector, leading the higher recorded SSE.

#### 4 Summary and Conclusions

During the development of THOR, NPL built a prototype instrument to identify optimal components and test their SSE sensitivities. A CVI Melles Griot lens was chosen as THOR's objective lens, having the lowest SSE of the lenses tested and suggesting that THOR's final SSE would be of the order of  $<6 \times 10^{-5}$ , when using a Lyot stop with a diameter slightly smaller than the theoretical optimum. The sensitivities of the SSE to the Lyot stop and collimating lens positions were also tested; small variations from optimum were not significant, although it was better for the Lyot stop to be slightly too far from the lens than too close. There was no measured increase in the radiometer's SSE when the collimating lens was moved towards the field stop; however, the SSE was seen to increase as the lens was moved away from the field stop.

The best SSE achieved during these preliminary tests was  $<6 \times 10^{-5}$ . During THOR's construction, some further compromises were required and the final instrument is expected to have a SSE of  $8 \times 10^{-5}$ . This compares to  $<5 \times 10^{-5}$  by Yoon et al. [9]. The effect of this in measuring the temperature of a HTFP depends on the relative radial radiance profiles of the calibration source and the HTFP furnace. When THOR is calibrated for spectral radiance responsivity, the calibration source will be a uniform, laser illuminated integrating sphere with a 3 mm aperture. The cell aperture has a 3 mm diameter, while the furnace is reasonably uniform to a diameter of  $\sim 6$  mm and then drops off rapidly. Initial calculations using the method described in [11] suggest that temperature measurements using THOR would require maximum corrections of 3 mK for Cu and 11 mK for Re-C to account for its SSE.

**Acknowledgments** The authors wish to acknowledge the advice that Howard Yoon of NIST provided in the initial stages of THOR's design. This work was funded by the UK National Measurement System.

© Crown copyright 2013. Reproduced by permission of the Controller of HMSO and Queen's printer for Scotland.

## References

1. M.R. Dury, T.M. Goodman, D.H. Lowe, G. Machin, E.R. Woolliams, in *Proceedings of Ninth International Temperature Symposium*, Los Angeles, *Temperature: Its Measurement and Control in Science and Industry*, vol. 8, ed. by C.W. Meyer, AIP Proceedings 1552 (AIP, Melville, NY, 2013), pp. 65–70
2. G. Machin, in *Proceedings of Ninth International Temperature Symposium*, Los Angeles, *Temperature: Its Measurement and Control in Science and Industry*, vol. 8, ed. by C.W. Meyer, AIP Proceedings 1552 (AIP, Melville, NY, 2013), pp. 305–316
3. G. Machin, P. Bloembergen, J. Hartmann, M. Sadli, Y. Yamada, *Int. J. Thermophys.* **28**, 1976 (2007)
4. G. Machin, K. Anhalt, P. Bloembergen, M. Sadli, Y. Yamada, E.R. Woolliams, in *Proceedings of Ninth International Temperature Symposium*, Los Angeles, *Temperature: Its Measurement and Control in Science and Industry*, vol. 8, ed. by C.W. Meyer, AIP Proceedings 1552 (AIP, Melville, NY, 2013), pp. 317–322
5. R. Winkler, E.R. Woolliams, W.S. Hartree, S.G.R. Salim, N.P. Fox, J.R. Mountford, M. White, S.R. Montgomery, *Int. J. Thermophys.* **28**, 2087 (2007)
6. E.R. Woolliams, M.R. Dury, T.A. Burnitt, P.E.R. Alexander, R. Winkler, W.S. Hartree, S.G.R. Salim, G. Machin, *Int. J. Thermophys.* **32**, 1 (2011)
7. H.W. Yoon, C.E. Gibson, G.P. Eppeldauer, A.W. Smith, S.W. Brown, K.R. Lykke, *Int. J. Thermophys.* **32**, 2217 (2011)
8. J. Hartmann, K. Anhalt, J. Hollandt, E. Schreiber, Y. Yamada, *Temperature 2003* (VDI Verlag GmbH, Berlin, 2003)
9. H.W. Yoon, D.W. Allen, R.D. Saunders, *Metrologia* **42**, 89 (2005)
10. G. Machin, R. Sergienko, in *Proceedings of TEMPMEKO 2001, 8th International Symposium on Temperature and Thermal Measurements in Industry and Science*, ed. by B. Fellmuth, J. Seidel, G. Scholz (VDE Verlag, Berlin, 2002), pp. 155–160
11. P. Saunders, *Int. J. Thermophys.* **32**, 1633 (2011)